https://doi.org/10.5194/egusphere-2024-2084
Preprint. Discussion started: 23 July 2024

Design Study for an Airborne N_2O Lidar

Christoph Kiemle, Andreas Fix, Christian Fruck, Gerhard Ehret, Martin Wirth

Deutsches Zentrum für Luft- und Raumfahrt (DLR), Institut für Physik der Atmosphäre, D-82234 Oberpfaffenhofen, Germany

Correspondence to: Christoph Kiemle (Christoph.Kiemle@dlr.de)

Abstract. Nitrous oxide (N_2O) is the third most important greenhouse gas modified by human activities after carbon dioxide and methane. This study examines the feasibility of airborne differential absorption lidar to quantify N_2O emissions from agriculture, fossil fuel combustion, industry and biomass burning. The mid-infrared spectral region, where suitably strong N_2O absorption lines exist, challenges passive remote sensing by means of spectroscopy due to both low solar and terrestrial radiation. Lidar remote sensing is principally possible thanks to the laser as independent radiation source, but has not yet been realized due to technological challenges. Mid-infrared N_2O absorption bands suitable for remote sensing are investigated. Simulations show that a spectral trough position between two strong N_2O lines in the 4.5 µm band is the best option. A second option exists in the 3.9 µm band at the cost of higher laser frequency stability constraints and less measurement sensitivity. Both options fulfill the N_2O measurement requirements for agricultural areal or point source emission quantification (0.5 % measurement precision, 500 m spatial resolution) with technically realizable and affordable transmitter (100 mW average laser power) and receiver (20 cm telescope) characteristics for integrated-path differential absorption lidar that measures the column concentration beneath the aircraft. While a satellite implementation is still out of reach owing to the lack of space-proof technology, the development of an airborne N_2O lidar is feasible, yet would benefit from progress in infrared laser transmitter and low-noise detection technology.

1 Introduction

The average concentration of nitrous oxide (N_2O) amounts to only 337 ppb yet its global warming potential is nearly 300 times that of CO_2 on a 100-year span (Arias et al., 2021). This makes N_2O the third most important greenhouse gas contributing to human-induced global warming after carbon dioxide and methane. The major anthropogenic source is nitrogen fertilization on arable land. Further N_2O sources are processes in the chemical industry and combustion processes. According to current knowledge, anthropogenic sources contribute ~36 % to total global N_2O emissions (Tian et al., 2024). Emissions from natural soils and oceans constitute the major natural source. Agricultural N_2O emissions are increasing due to interactions between nitrogen inputs and global warming, constituting an emerging positive N_2O-climate feedback. The recent increase in global N_2O emissions exceeds even the most pessimistic emission trend scenarios developed by the IPCC, underscoring the urgency to mitigate N_2O emissions (Tian et al., 2024). Estimating N_2O emissions from agriculture is inherently complex and comes with a high degree of uncertainty, due to variability in weather and soil characteristics, in

https://doi.org/10.5194/egusphere-2024-2084
Preprint. Discussion started: 23 July 2024

agricultural management options and in the interaction of field management with environmental variables (Eckl et al., 2021). Moreover, N_2O measurements are sparse. Consequently, more comprehensive N_2O concentration measurements are needed, particularly by means of remote sensing. Recently, the World Meteorological Organization has launched the Global Greenhouse Gas Watch (G3W) initiative to endorse, among others, this need (WMO, 2024).

The mid-infrared (mid-IR) spectral region, where suitably strong N_2O absorption lines exist, challenges passive remote sensing by means of spectroscopy due to both low solar and terrestrial radiation. Lidar remote sensing is principally possible thanks to the laser as independent radiation source, but has not yet been realized due to technological challenges. While mid-IR lidars are employed for ground-based pollution detection (e.g., Robinson et al., 2011; Gong et al., 2020), to our knowledge, neither an airborne N_2O lidar has been realized yet, nor has passive remote sensing by means of spectroscopy been used to measure N_2O concentrations in the lower troposphere.

Airborne N_2O lidar remote sensing will combine the advantages of high measurement accuracy, large-area coverage and dawn/dusk or nighttime measurement capability. Initial studies have shown that Integrated-Path Differential-Absorption (IPDA) lidar from an airborne or even a satellite platform has the potential to measure N_2O with high precision and low bias (Ehret and Kiemle, 2005; Ehret et al., 2008). It uses the Earth surface backscatter signal at an "online" laser wavelength tuned to a N_2O absorption line to obtain column concentrations of N_2O (Ehret et al., 2008; Amediek et al., 2017). A parallel reference measurement at the non-absorbed "offline" wavelength avoids biases generated by albedo variations or aerosol layers within the light path. In comparison to conventional lidar using backscatter from atmospheric molecules and aerosol, IPDA lidar yields high signal to noise ratio at comparatively low instrument size since the surface backscatter is stronger. Still, accurate ranging by means of short laser pulses is important for precise measurements of the individual column length. First airborne systems for CO_2 and CH_4 have demonstrated high measurement accuracy and the capability to measure in broken cloud environments (Amediek et al., 2017; Barton-Grimley et al., 2022; Mao et al., 2024).

The objective to quantify agricultural areal or point source emissions requires obtaining N_2O column concentration gradients along the flight track between background levels outside the emission regions and the N_2O source regions, cultivated soils or exhaust plumes from, e.g., fertilizer production sites. The airborne lidar should point downward from a flight altitude of about 5 km, well above the boundary layer in which N_2O surface emissions disperse vertically by turbulence. Gradients over agricultural regions measured by airborne in-situ instruments (Eckl et al., 2021; Waldmann et al., 2024) suggest that the maximum uncertainty of the N_2O column measurement should be 0.5 % and that an along-track horizontal measurement resolution of 500 m is sufficient. To detect smaller but denser N_2O emission plumes from industrial production sites the horizontal resolution can be improved at the cost of precision. Lidar allows such tradeoffs to adapt to the measurement objectives.

This study first investigates the N_2O spectroscopy to find suitable absorption lines. The chosen wavelength has consequences for the surface reflectance, the atmospheric absorption, the solar and terrestrial background radiation, as well as transmitter and detector options. All relevant environment, instrument and spectroscopic constraints are implemented into a lidar

https://doi.org/10.5194/egusphere-2024-2084
Preprint. Discussion started: 23 July 2024

simulation model to design the instrument in order to meet the above measurement requirements. Finally, although beyond the scope of this study, ideas for suitable lidar transmitter and detector technologies are briefly discussed.

2 N_2O Spectroscopy

Up-to-date spectroscopic data retrieved with the HITRAN (high resolution transmission molecular absorption database) Application Programming Interface (HAPI) are used to find suitable absorption lines in the four major rotational-vibrational N_2O bands located at 2.9, 3.9, 4.5 and 7.8 µm (Nemtchinov et al., 2004; Loos et al., 2015; Kochanov et al., 2016; Gordon et al., 2022). Molecular absorption cross sections are calculated line-by-line with a resolution of 0.001 cm^{-1} with the Hartmann-Tran scheme (Ngo et al., 2013) using standard atmosphere profiles of pressure, temperature and trace gas concentrations within the lowest 5 km, below the foreseen flight altitude. The vertically integrated product of the absorption cross section σ and the trace gas molecule number density n, both varying with altitude z between the surface sfc and the flight height flh, is the optical depth od:

$$od_{gas} = \int_{sfc}^{flh} \sigma_{gas}(z)\, n_{gas}(z)\, dz \quad (1)$$

It is related to atmospheric transmission and represents the spectroscopic determining parameter for IPDA lidar column measurements. The IPDA technique is well described in e.g. Ehret et al. (2008) and Amediek et al. (2017). Criteria for line selection are (a) appropriate line strength, related to the optimal optical depth, (b) low temperature sensitivity and (c) minimal influence by other gases. The optimal line strength or optical depth is a compromise between too weak absorption and saturation. The optimal optical depth typically lies between 0.5 and 1.2 and depends on column height and instrument noise (Ehret et al., 2008). Temperature sensitivity is determined using an atmospheric temperature profile shifted by 1 K and evaluating the difference in optical depth between the reference and the temperature-shifted optical depth.

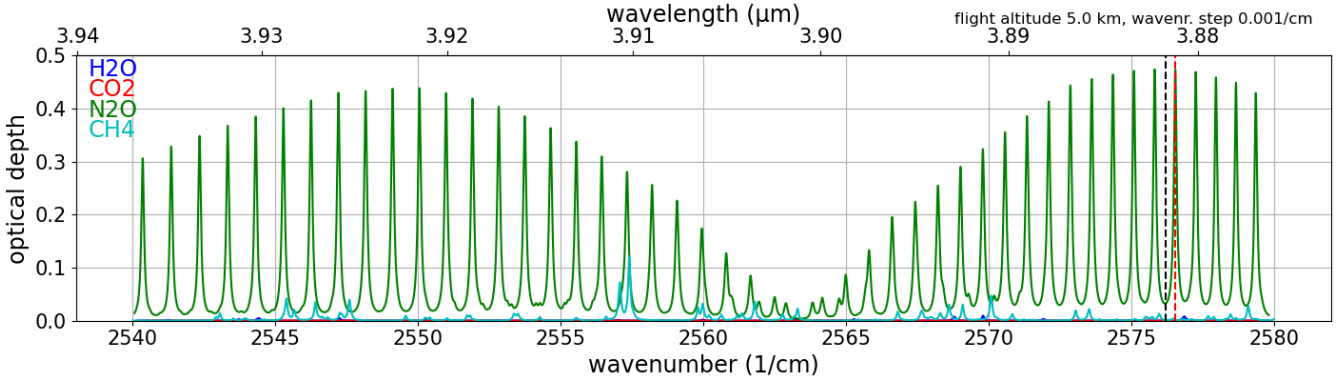

Figure 1: ***Optical depth spectrum of trace gases in the 3.9 µm N_2O band in a standard atmosphere vertical column covering the lowest 5 km. The selected online (offline) position is highlighted in red (black). Absorption lines of N_2O (green), water (blue), CO_2 (red) and CH_4 (cyan) need to be considered in this spectral region.***

https://doi.org/10.5194/egusphere-2024-2084
Preprint. Discussion started: 23 July 2024

The N_2O bands at 2.9 and 3.9 µm contain absorption lines of comparable strength, yet the entire 2.9 µm N_2O band is dominated by water vapor absorption lines whose wings are without exception stronger than the N_2O lines within the lowest 5 km, hence the 2.9 µm band is not shown here. The 3.9 µm N_2O band is illustrated in Fig. 1 showing the one-way column optical depth of the lowermost 5 km as function of vacuum wavenumber and wavelength. The 3.9 µm band is composed of relatively weak lines suitable for satellite lidar (Ehret and Kiemle, 2005; Ehret et al., 2008) yet suboptimal for lower tropospheric concentration measurements. One of the strongest absorption lines, situated at 2576.54 cm^{-1}, is selected here (red line), characterized by both low influence of other absorbing gases and low temperature sensitivity. The offline reference wavenumber is set to a neighboring minimum absorption and temperature sensitivity position.

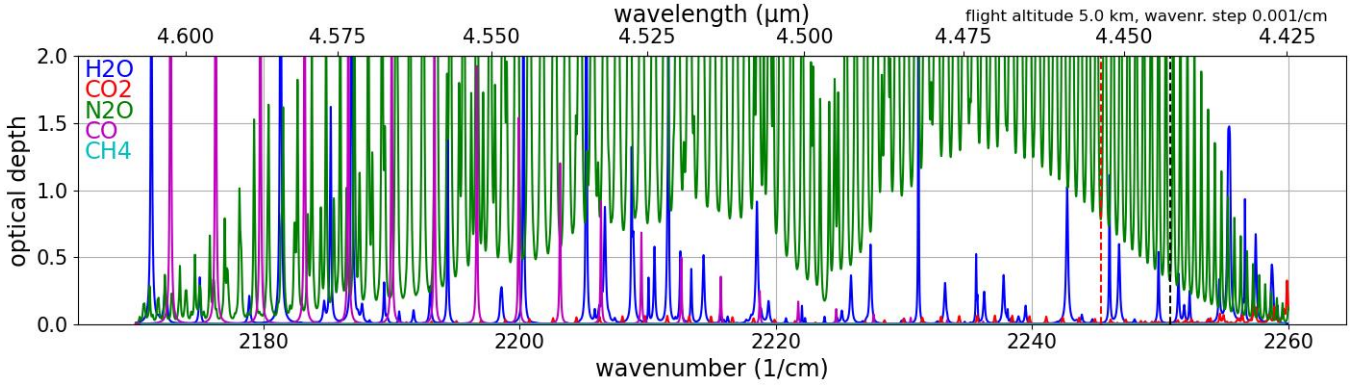

Figure 2: ***Optical depth spectrum of trace gases in the 4.5 µm N_2O band in a standard atmosphere vertical column covering the lowest 5 km. The selected online (offline) position is highlighted in red (black) at the right. Absorption lines of CO have to be considered in addition (magenta).***

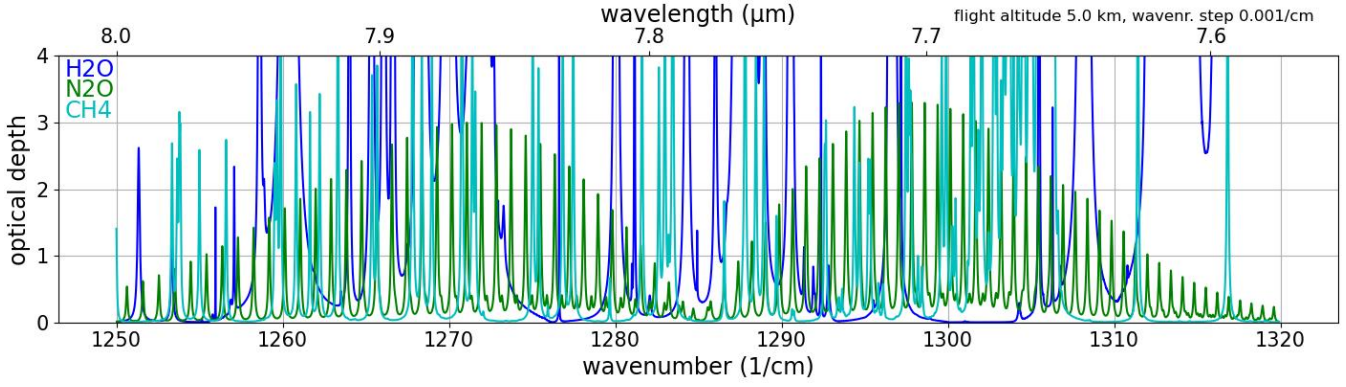

Figure 3: ***Optical depth spectrum of trace gases in the 7.8 µm N_2O band, as is Figures 1 and 2. The atmospheric window ends at 1310 cm^{-1} where a large water vapor absorption band begins.***

https://doi.org/10.5194/egusphere-2024-2084
Preprint. Discussion started: 23 July 2024

The 4.5 µm band contains much stronger N_2O lines (Fig. 2). N_2O lines with suitable strength exist at both edges of the band, around 2180 and 2255 cm^{-1}, as well as in the center of the band. However, all of those reveal inappropriate due to overlapping water lines and high temperature sensitivity in the center of the band. Finally, Figure 3 illustrates the 7.8 µm band which is so densely populated with strong water and methane lines that no suitable N_2O line candidate is found. Water vapor is difficult to correct due to its high variability in the lower troposphere. Consequently, we restrict this study to the 3.9 and 4.5 µm N_2O bands. In the 4.5 µm band, trough positions at minimum optical depth in between two strong lines can be selected for both on- and offline, as used for CH_4 lidar and foreseen for MERLIN, the Remote Sensing Methane Lidar Mission (Kiemle et al., 2011; Amediek et al., 2017). A trough position has two advantages. First, it relaxes the laser frequency stability requirement due to a relatively flat optical depth in the center of the trough. Second, the measurement sensitivity at low altitudes, i.e. near the surface where the N_2O sources are located, is improved thanks to pressure broadening of both lines surrounding the trough (Ehret et al., 2008). Figure 4 illustrates the differences in sensitivity between line center, wing and trough (i.e. far wing) positions. Within the lowest 1 km a spectral position in the center of the trough is found to increase the near-surface sensitivity to N_2O by about a factor of 1.5 (= 1.4 % / 0.92 %) in comparison to a line center position.

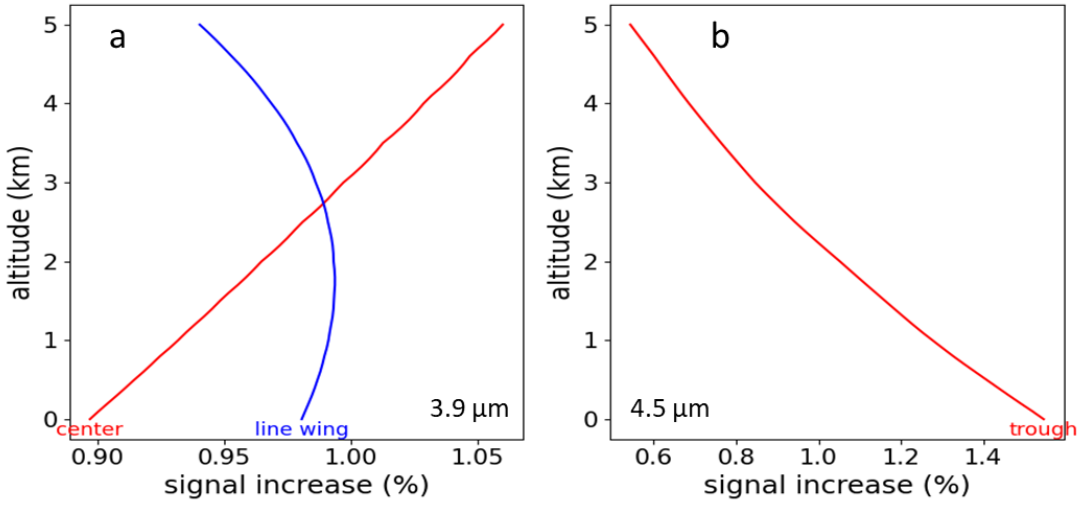

Figure 4: ***N_2O measurement sensitivity expressed as online optical depth (signal) increase under the assumption of a hypothetical 50 % N_2O concentration increase within a 100 m thick layer, as function of the altitude of this layer. A) 3.9 µm line center (red) position of Fig. 1 in comparison with an online line wing (blue) position at 2576.57 cm^{-1} (very close to the line center; not further discussed). B) 4.5 µm online trough position of Fig. 2.***

https://doi.org/10.5194/egusphere-2024-2084
Preprint. Discussion started: 23 July 2024

Therefore, in the 4.5 µm band we select a trough position at the high-wavenumber side of the band at 2245.35 cm^{-1} because it is less influenced by other gases than the low-wavenumber side (Fig. 2). The closest possible offline position is at 2250.75 cm^{-1}. The 10.7 nm distance from the online position may require separate lasers for the generation of the on- and offline wavelengths and may lead to uncertainties estimated to < 1 % if surface albedo or aerosol extinction are wavelength dependent (Amediek et al., 2009). Table 1 summarizes the spectroscopic characteristics of both band selections. The temperature sensitivity is sufficiently low, especially at the online positions. The additional optical depth by line wings of other gases is insignificant at 3.9 µm and ~0.01 at 4.5 µm. In the event of a 50 % concentration change possible for H_2O yet very unlikely for CO_2, the impact on the total optical depth at 4.5 µm would be 0.005/0.79 ≈ 0.6 % for the online and 0.005/0.34 ≈ 1.5 % for the offline, which we consider uncritical. Note that our line selection is provisional as new spectroscopic data may lead to better options.

Line selection	**wavenumber cm^{-1}**	**N_2O opt. depth (0-5 km)**	**temperature sensitivity**	**opt. depth of other gases (0-5 km)**
3.9 µm online, line center	2576.54	0.47	- 0.01 % / K	0.002 (CH_4)
3.9 µm offline	2576.20	0.03	0.43 % / K	0.001 (CH_4)
4.5 µm online, trough	2245.35	0.78	0.06 % / K	0.008 (H_2O)
4.5 µm offline	2250.75	0.33	- 0.31 % / K	0.008 (H_2O), 0.010 (CO_2)

Table 1: ***Selected online and offline spectral positions in the 3.9 and 4.5 µm N_2O absorption bands with corresponding N_2O optical depth for a vertical standard atmosphere column in the lowest 5 km, relative N_2O optical depth change per Kelvin temperature change, and optical depth of other trace gases.***

3 Mid-IR Surface Albedo, Aerosol Influence and Background Radiation

The albedo is key for IPDA lidar which relies on surface backscatter intensity. It is generally low in the IR, compared to the near-IR and visible spectral ranges. Ehret and Kiemle (2005) and Ehret et al. (2008) used a value of 0.02 (2 %) for both land and water surfaces. The Ecosystem Spaceborne Thermal Radiometer Experiment on Space Station (ECOSTRESS) spectral library contains a limited set of mid-IR reflectance data (Baldridge et al., 2009; Meerdink et al., 2019). Table 2 lists their agriculturally relevant values. We keep the small value of 2 % from our initial studies for the present simulation which can be considered a safe worst case. Over agricultural soils, extinction by rural aerosol within the boundary layer is expected. Based on IR lidar measurements by Vaughan et al. (1995 and 1998) and scaled to 3.9 and 4.5 µm using an Angström exponent of 1, we assume a worst-case maximum aerosol optical depth of 0.2 across the lowest 5 km. The Rayleigh optical depth due to air molecular extinction amounts to ~$2 \cdot 10^{-5}$ at around 4 µm in the lowest 5 km and is therefore negligible.

https://doi.org/10.5194/egusphere-2024-2084
Preprint. Discussion started: 23 July 2024

Photons from solar scattered and terrestrial emitted radiation cause noisy background signals in the detector. The mid-IR radiation emitted from earth's surface is calculated with Planck's law (Stull, 2017) assuming a blackbody with albedo zero and no atmosphere. According to Kirchhoff's law this represents the worst-case maximum terrestrial radiation, also because the atmosphere is mostly colder than earth's surface. The solar radiation is calculated with Planck's law assuming an albedo of 0.4, a sun in the zenith and no atmosphere, which also represents a maximum-radiation worst case. Table 2 summarizes the environmental boundary conditions for the lidar simulation. The low total radiation, close to the spectral minimum of the sum of terrestrial emitted and solar scattered radiation represents a challenge for passive remote sensing in the mid-IR.

N_2O band	**3.9 µm**	**4.5 µm**	**unit**	**remarks**
Albedo	0.03-0.04	**0.02**-0.03	-	over grain or grass
	0.23-0.32	0.13-0.35		over soil
Aerosol optical depth, od_a	0.2	0.2	-	0 - 5 km
Earth emission	0.4	1.0	W / (m^2 µm sr)	albedo 0.0 assumed
Solar backscatter	1.2	0.8	W / (m^2 µm sr)	albedo 0.4 assumed
Total background radiation	1.6	1.8	W / (m^2 µm sr)	sum of terrestrial emitted and solar scattered radiation
N_2O $od_{on} - od_{off}$	0.44	0.45	-	see Eqs. (1) and (3)

Table 2: ***Mid-IR albedo, aerosol optical depth and background radiation used for the N_2O lidar simulation. The minimum albedo of 0.02 (bold) is selected as a worst case for the simulation. Soil has about ten times higher albedo than grain or grass. The differential absorption optical depth is about equal in both N_2O bands.***

4 N_2O Lidar Simulation

The airborne lidar performance is assessed by implementing the measurement requirements together with environmental, instrumental and spectroscopic constraints into a lidar noise propagation model developed for earlier studies (Kiemle et al., 2011 and 2017). Atmospheric transmission and surface scattering are evaluated to compute the backscattered signal power as function of emitted laser power P_L, surface reflectance ρ (= albedo / π), receiver optical efficiency η, telescope area A, and range R (= 5 km) for the on- and offline wavelengths in the IPDA lidar equation:

$$P_{on,off} = P_{L,on,off}\, \varrho\, \eta\, A\, R^{-2}\, exp^{-2\,(od_a + od_{on,off})} \quad (2)$$

According to the Beer-Lambert law the exponential term represents the atmospheric transmission along the vertical path, lowered by the aerosol optical depth od_a and the N_2O on- and offline optical depths. Solving Eq. (2) for the respective on- and offline optical depths, and assuming constant surface albedo, optical efficiency, and aerosol optical depth for both on-

https://doi.org/10.5194/egusphere-2024-2084
Preprint. Discussion started: 23 July 2024

and offline wavelengths, we obtain the differential absorption optical depth DAOD from subtracting the offline solution of Eq. (2) from the online solution:

$$DAOD = od_{on} - od_{off} = \frac{1}{2} ln\left(\frac{P_{off}/E_{off}}{P_{on}/E_{on}}\right), \quad (3)$$

where E_{on} and E_{off} are energy reference measurements accounting for variations of the pulse energy or power, P_L. After Eq. (1) the DAOD is proportional to the N_2O column concentration weighted with the absorption cross section. Table 2 lists the DAOD values expected in a reference atmosphere.

Simulation parameter	**value**	**reference**
Requirements: flight altitude	**5 km**	Eq. (2): R
horizontal along-track resolution	**500 m**	
aircraft velocity	150 m/s	
Laser: **average IR online and offline power**	**100 mW**	Eq. (2): $P_{L,on,off}$
pulse energy	0.5 mJ	
pulse energy reference measurement precision	1 %	Eq. (3): $E_{on,off}$; Ehret et al. (2008)
double pulse (online, offline) repetition rate	100 Hz	
number of averaged double pulses	333	
pulse length	15 ns	Ehret et al. (2008)
Receiver: **telescope area**	**0.03 m²**	Eq. (2): A (20 cm diam.)
telescope focal ratio, 1/f	1.25	
optical efficiency	**0.65**	Eq. (2): η; Kiemle et al. (2011)
optical narrow-band filter	1 nm	Ehret et al. (2008)
field-of-view, full-angle	0.8 mrad	
footprint size at surface	4 m	
Detector: MCT APD, NEP	**0.1 pW/Hz$^{0.5}$**	e.g., Sun et al. (2017)
diameter	200 µm	e.g., Martyniuk et al. (2023)
bandwidth	3 MHz	Ehret et al. (2008)
Surface albedo	**0.02**	Eq. (2): ρπ; Ehret et al. (2008)

Table 3: ***N_2O lidar instrument parameters assumed for the simulation, partly adopted from earlier studies and regarded as achievable. Parameters of first importance to the performance are in bold.***

https://doi.org/10.5194/egusphere-2024-2084
Preprint. Discussion started: 23 July 2024

Table 3 lists the major instrument parameters. The larger the average laser power, surface reflectance (albedo), and telescope size, the stronger the received signal power and consequently the signal-to-noise ratio (SNR). Further parameters influencing the SNR are the flight altitude, the horizontal resolution, the laser pulse repetition rate, the receiver field-of-view and several detector parameters. Parametric analyses allow to finetune the instrument with the aim to optimize efficiency or flexibility. Parameters can depend on each other, such as the aircraft velocity, the horizontal resolution, the repetition rate, and the number of averaged pulses. Likewise, for the laser, repetition rate, pulse energy and average laser power are related. Finally, the telescope field-of-view is related to its diameter, its focal ratio, and the detector size. Equations implement all relevant dependencies in the model. For more details we refer to our former studies (Ehret et al., 2008; Kiemle et al., 2011 and 2017).

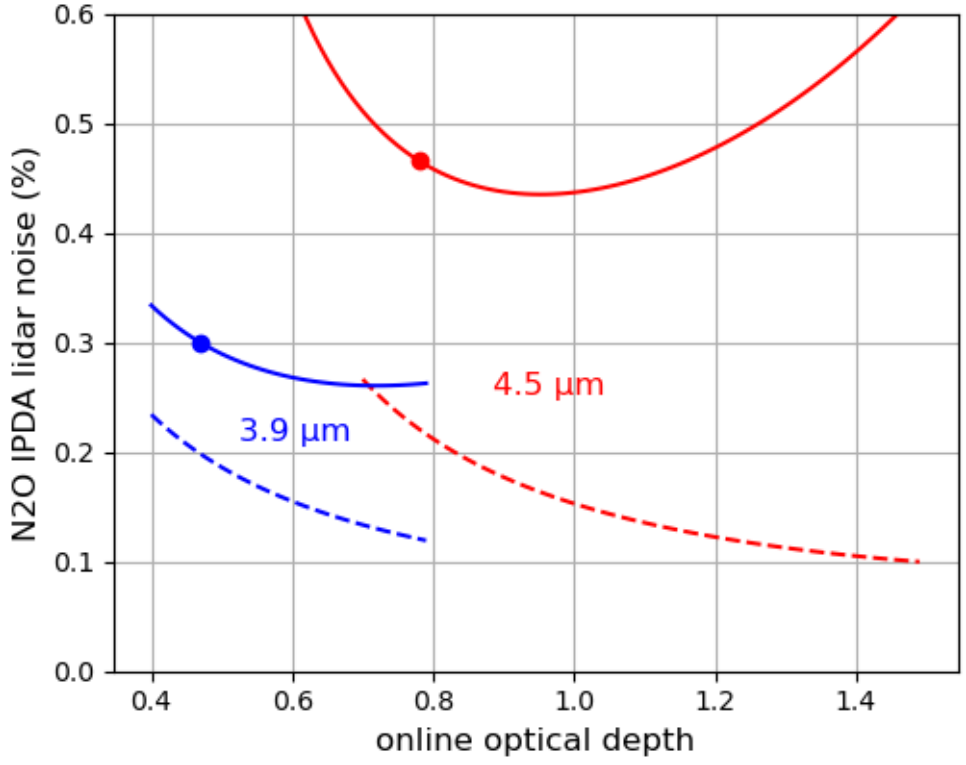

Figure 5: Simulated N_2O lidar measurement precision at 3.9 (blue) and 4.5 µm (red) as function of online optical depth under the conditions of Tables 2 and 3. The dots indicate the selections of Table 1 and the dashed lines represent an ideal noise-free detector for comparison. The absence of strong lines in the 3.9 µm band limits the 3.9 µm online optical depth range.

The simulation is run with the environment conditions of Table 2 and the instrument parameters of Table 3. All noise contributors, Poisson noise from laser photons and background radiation, detector noise, laser speckle noise within the field of view, and energy reference measurement noise are uncorrelated. Thus, error propagation on the basis of Eqs. (2) and (3)

https://doi.org/10.5194/egusphere-2024-2084
Preprint. Discussion started: 23 July 2024

provides the overall one-sigma precision of the N_2O measurements as function of the prescribed online optical depth for both N_2O bands (Fig. 5). The offline optical depth is kept at a constant level of 0.03 (0.33) at 3.9 (4.5) µm. At 3.9 µm this level corresponds to a representative minimum optical depth within the band (Fig. 1), while at 4.5 µm the offline from Table 1 may serve several neighboring online trough options (Fig. 2). The dashed lines show the performance of an ideal noise-free detector for comparison. Their minima are right-shifted because the optimum online optical depth is larger under low-noise conditions (Ehret et al., 2008). The curves are flatter since a low-noise instrument is more tolerant with respect to suboptimal spectroscopic settings.

Assuming, as a provisional proxy, a mercury cadmium telluride (MCT) avalanche photodiode (APD) detector with a noise equivalent power (NEP) of 0.1 $pW/Hz^{1/2}$, the optimum online optical depth for minimum noise is around 0.7 (0.9) for 3.9 (4.5) µm. Due to the lack of more comprehensive mid-IR detector data the NEP is estimated on the basis of near-IR realizations and mid-IR prototypes (Sun et al., 2017; Martyniuk et al., 2023) using large security margins, likely representing a worst case. The absence of strong lines in the 3.9 µm band (Fig. 1) prevents an optimum online setting yet the low offline optical depth of 0.03 provides satisfying low-noise levels (Fig. 5). At 4.5 µm, a trough nearby the optimum optical depth could be selected (Fig. 2). Stronger neighboring troughs that would fit the optimum suffer from overlapping water line wings and larger temperature sensitivity. The 4.5 µm selection also allows for a measurement precision fulfilling the initial requirement of 0.5 %, although at a higher noise level, primarily due to the relatively high offline optical depth of 0.33. Away from the optimum, noise increases towards lower optical depths because of a smaller DAOD (Eq. 3), and towards higher optical depths because of online signal saturation.

In addition to uncorrelated random noise which averages out over longer data accumulation lengths, persisting systematic uncertainties (biases) may arise from errors in the spectroscopic parameters. The HITRAN database specifies the N_2O line intensity uncertainties to within 2 and 5 %. This does not threaten the objectives to quantify agricultural areal or point source emissions since those are derived from relative column gradients between sources and background rather than from absolute measurements. In addition, spectroscopy errors can be corrected by comparing the lidar columns against collocated profiles from high accuracy aircraft in-situ sensors (Amediek et al., 2017; Mao et al., 2024). Biases may also arise from variability in the actual aerosol, temperature and pressure profiles within the columns. Experience and simulation (Ehret et al., 2008; Kiemle et al., 2011; Amediek et al., 2017) shows that these usually remain below 1 %. Finally, albedo variations cause measurement uncertainties if the on- and offline surface laser spots are not fully overlapping, which is generally the case. Those however tend to behave like random deviations leading to slightly increased noise levels (Amediek et al., 2009).

5 Technology Options and Readiness

IR lidar transmitters that can be considered for the described purpose are (a) tunable solid-state lasers such as transition-metal (TM)-doped II-VI chalcogenide lasers, for example Fe:ZnS or Fe:ZnSe lasers, (b) optical parametric oscillators (OPO) and amplifiers, and (c) laser sources based on nonlinear difference frequency generation (DFG; Robinson et al., 2011) or

https://doi.org/10.5194/egusphere-2024-2084
Preprint. Discussion started: 23 July 2024

Raman shifting. Using OPOs, wavelengths in the 3.9 to 4.5-µm range are readily accessible. When pumping with the ubiquitous Nd:YAG laser at 1.064 µm, the corresponding signal wavelengths that lead to an idler wavelength at 3.9 or 4.5 µm are ~1.46 or 1.39 µm, respectively. This requires suitable nonlinear crystals with transparency at all these wavelengths. But, other pump laser sources at longer wavelength, cascaded OPOs or DFG sources are also options (e.g. DFG of 1.064 µm with 1.46 µm results in 3.9 µm and mixing 1.064 µm with 1.39 µm results in 4.5 µm, respectively).

Low-noise and high-bandwidth radiation detection is a challenge in the mid-IR. Prototype MCT APDs can achieve very low excess noise in the mid-IR, yet cooling down to at least 200 K is required to reduce dark currents, and the detector linear analog output spans a dynamic range of only 2-3 orders of magnitude (Sun et al., 2017). Developments are ongoing but manufacturability is considered low (Chen et al., 2021; Martyniuk et al., 2023). In addition, the literature reveals that efforts go into the development of imaging sensors, while lidar requires a single sensor with a large photosensitive area in order to satisfy optical constraints (cf. Table 3). Due to the lack of data we used in our study a conservative approach for the simulation, with a large security margin for the detector noise on the basis of data from near-IR realizations and mid-IR prototypes. An alternative to MCT is indium antimonide (InSb), yet mid-IR InSb APDs apparently have more noise and less bandwidth (Abautret et al., 2015; Alimi et al., 2020). Besides APD detectors, up-conversion detectors (UCD; Hoegstedt et al., 2016; Meng et al., 2018) or superconducting nanowire single-photon detectors (SNSPD; Charaev et al., 2023) could offer high-efficiency, low-noise signal detection. Also, in this area, developments are underway.

Concerning methodical alternatives for active remote sensing, the more common differential absorption lidar (DIAL) technique exploits atmospheric instead of surface backscatter with the advantage of providing vertical profiles of trace gases instead of column concentrations. A dedicated simulation using the same lidar simulator shows that this is at the expense of a 100 times larger laser power and telescope aperture product ($P_L \cdot A$ = 0.3 W m^2 instead of 0.003 W m^2 from Table 3) to compensate for the much weaker atmospheric backscatter signals, even within a boundary layer with rural aerosol. A low-power alternative is IPDA or DIAL with heterodyne instead of direct signal detection. It requires a diffraction-limited optical setup and laser pulse repetition rates in the kHz range to manage speckle-induced noise. So far, ground-based profiling systems (Koch et al., 2008; Yu et al., 2024) and an airborne realization (Spiers et al., 2011; Jacob et al., 2019) for CO_2 have been reported, yet only in the near-IR. Another low-power option for IPDA is (modulated) continuous-wave (cw) laser operation instead of emitting short pulsed signals. For measurements with a precision requirement below 1 % however, the length of the atmospheric column must be known to an accuracy of a few meters which is only practicable with short laser pulses in combination with a sufficiently large detection bandwidth (Table 3; Ehret et al., 2008). Alternatively, a precision range finder had to be added which annihilates the cost benefit of cw lidar. We conclude that methodical alternatives for N_2O active remote sensing are either too expensive, or their maturity for airborne operation lags behind that of direct detection pulsed IPDA.

https://doi.org/10.5194/egusphere-2024-2084
Preprint. Discussion started: 23 July 2024

6 Conclusion

With a resulting noise level of < 0.5 % our IPDA lidar design fulfills the measurement requirements for N_2O regional gradient or hot spot detection with technically realizable and affordable transmitter (100 mW average laser power) and receiver (20 cm telescope, MCT APD) characteristics. The simulation results show better performance at 3.9 µm in terms of the noise level. However, the trough position at 4.5 µm yields higher measurement sensitivity at low altitudes and considerably relaxes the laser frequency stability requirement. This is therefore the preferred option. In case the 11 nm distant offline position is inacceptable, or other issues at 4.5 µm appear, the 3.9 µm alternative is the fallback option. The simulation tool will be applied to trade off various instrument options as technology is developing. Better low-noise IR detectors will be particularly beneficial. While a satellite implementation is not impossible, but still far away because of lacking space-proof technology, the development of an airborne N_2O lidar at 3.9 or 4.5 µm is recommended given the technical feasibility and the scientific-societal need.

Code/Data availability

Code and data can be provided by the first author on request.

Author contribution

CK developed the model code, performed the simulations, and prepared the manuscript with contributions from all co-authors. AF, CF, GE and MW contributed information on available laser and detector technology.

Competing interests

The authors declare that they have no conflict of interest. CK is member of the editorial board of AMT.

References

Abautret, J., Perez, J. P., Evirgen, A., Rothman, J., Cordat, A., Christol, P.: Characterization of midwave infrared InSb avalanche photodiode. J. Appl. Phys., 117 (24): 244502, doi:10.1063/1.4922977, 2015.

Alimi, Y., Pusino, V., Steer, M. J., and Cumming, D. R. S.: InSb Avalanche Photodiodes on GaAs Substrates for Mid-Infrared Detection, IEEE Transactions on Electron Devices, 67, 1, 179-184, doi: 10.1109/TED.2019.2956283, 2020.

Amediek, A., Fix, A., Ehret, G., Caron, J., and Durand, Y.: Airborne lidar reflectance measurements at 1.57 µm in support of the A-SCOPE mission for atmospheric CO2, Atmos. Meas. Tech., 2, 755–772, doi:10.5194/amt-2-755-2009, 2009.

Amediek, A., Ehret, G., Fix, A., Wirth, M., Büdenbender, C., Quatrevalet, M., Kiemle, C., and Gerbig, C.: CHARM-F - a new airborne integrated-path differential-absorption lidar for carbon dioxide and methane observations: measurement performance and quantification of strong point source emissions, Applied Optics, 56 (18), 5182-5197, doi: 10.1364/AO.56.005182, 2017.

https://doi.org/10.5194/egusphere-2024-2084
Preprint. Discussion started: 23 July 2024

Arias, P.A. et al.: Technical Summary. In Climate Change 2021: The Physical Science Basis. Contribution of Working Group I to the Sixth Assessment Report of the Intergovernmental Panel on Climate Change, Cambridge University Press, Cambridge, United Kingdom and New York, USA, pp. 33−144. doi:10.1017/9781009157896.002, 2021.

Baldridge, A. M., Hook, S. J., Grove, C. I. and Rivera, G.: The ASTER Spectral Library Version 2.0, Remote Sensing of Environment, 113, 711-715, 2009.

Barton-Grimley, R. A., Nehrir, A. R., Kooi, S. A., Collins, J. E., Harper, D. B., Notari, A., Lee, J., DiGangi, J. P., Choi, Y., and Davis, K. J.: Evaluation of the High Altitude Lidar Observatory (HALO) methane retrievals during the summer 2019 ACT-America campaign, Atmos. Meas. Tech., 15, 4623–4650, doi:10.5194/amt-15-4623-2022, 2022.

Charaev, I., Bandurin, D. A., Bollinger, A. T., Phinney, I. Y., Drozdov, I., Colangelo, M., Butters, B. A., Taniguchi, T., Watanabe, K., He, X., Medeiros, O., Božović, I., Jarillo-Herrero, P., and Berggren, K. K.: Single-photon detection using high-temperature superconductors, Nature Nanotechnol. 18, 343-349, 2023.

Chen, J., Chen, J., Li, X. et al. High-performance HgCdTe avalanche photodetector enabled with suppression of band-to-band tunneling effect in mid-wavelength infrared, Nature npj Quantum Mater. 6, 103, doi:10.1038/s41535-021-00409-3, 2021.

Eckl, M., Roiger, A., Kostinek, J., Fiehn, A., Huntrieser, H., Knote, C., Barkley, Z. R., Ogle, S., Baier, B. C. Sweeney, C. and Davis, K. J.: Quantifying nitrous oxide emissions in the U.S. Midwest - A top-down study using high resolution airborne in situ observations, Geophys. Res. Lett., 48 (5), doi: 10.1029/2020GL091266, 2021.

Ehret, G. and Kiemle, C.: Requirements Definition for Future DIAL Instruments, ESA Study Final Report, ESA-CR(P)-4513, ESA Contract no. 10880/03/NL/FF, 2005.

Ehret, G., Kiemle, C., Wirth, M., Amediek, A., Fix, A., and Houweling, S.: Space-borne remote sensing of CO2, CH4, and N2O by integrated path differential absorption lidar: a sensitivity analysis, Appl. Phys. B 90, 593-608, 2008.

Gong, Y., Bu, L., Yang, B., Mustafa, F.: High Repetition Rate Mid-Infrared Differential Absorption Lidar for Atmospheric Pollution Detection, Sensors, 20, 2211, doi:10.3390/s20082211, 2020.

Gordon, I. E., Rothman, L. S., Hargreaves, R. J., Hashemi, R., Karlovets, E. V., Skinner, F. M., et al.: The HITRAN2020 molecular spectroscopic database, J. Quant. Spectrosc. Radiat. Transfer, 277, 107949, doi:10.1016/j.jqsrt.2021.107949, 2022.

Hoegstedt, L., Fix, A., Wirth, M., Pedersen, C., and Tidemand-Lichtenberg, P.: Upconversion-based lidar measurements of atmospheric CO2, Optics Express 24, 5, doi:10.1364/OE.24.005152, 2016.

Jacob, J. C., Menzies, R. T. and Spiers G. D.: Data Processing and Analysis Approach to Retrieve Carbon Dioxide Weighted-Column Mixing Ratio and 2-µm Reflectance With an Airborne Laser Absorption Spectrometer, IEEE Transactions on Geoscience and Remote Sensing, 57, 2, 958-971, doi:10.1109/TGRS.2018.2863711, 2019.

Kiemle, C., Quatrevalet, M., Ehret, G., Amediek, A., Fix, A., and Wirth, M.: Sensitivity studies for a space-based methane lidar mission, Atmos. Meas. Tech., 4, 2195-2211, doi:10.5194/amt-4-2195-2011, 2011.

https://doi.org/10.5194/egusphere-2024-2084
Preprint. Discussion started: 23 July 2024

Kiemle, C., Ehret, G., Amediek, A., Fix, A., Quatrevalet, M., and Wirth, M.: Potential of Spaceborne Lidar Measurements of Carbon Dioxide and Methane Emissions from Strong Point Sources, Remote Sens. 9, 1137, doi:10.3390/rs9111137, 2017.

Koch, G. J., Beyon, J. Y., Gibert, F., Barnes, B. W., Ismail, S., Petros, M., Petzar, P. J., Yu, J., Modlin, E. A., Davis, K. J., and Singh, U. N.: Side-line tunable laser transmitter for differential absorption lidar measurements of CO2: design and application to atmospheric measurements, Appl. Opt. 47, 944-956, 2008.

Kochanov, R.V., Gordon, I.E., Rothman, L.S., Wcislo, P., Hill, C., and Wilzewski, J.S.: HITRAN Application Programming Interface (HAPI): A comprehensive approach to working with spectroscopic data, J. Quant. Spectrosc. Radiat. Transfer, 177, 15-30, 2016.

Loos, J., Birk, M., Wagner, G.: Pressure broadening, -shift, speed dependence and line mixing in the ν3 rovibrational band of N2O, J. Quant. Spectrosc. Radiat. Transfer 150, 300-309, 2015.

Mao, J., Abshire, J. B., Kawa, S. R., Sun, X., and Riris, H.: Airborne lidar measurements of atmospheric CO2 column concentrations to cloud tops made during the 2017 ASCENDS/ABoVE campaign, Atmos. Meas. Tech., 17, 1061–1074, doi:10.5194/amt-17-1061-2024, 2024.

Martyniuk, P., Wang, P., Rogalski, A., Gu, Y., Jiang, R., Wang, F., Hu, W.: Infrared avalanche photodiodes from bulk to 2D materials, Light: Science & Applications 12:212, doi:10.1038/s41377-023-01259-3, 2023.

Meng, L., Fix, A., Wirth, M., Hoegstedt, L., Tidemand-Lichtenberg, P., Pedersen, C., and Rodrigo, P. J.: Upconversion detector for range-resolved DIAL measurement of atmospheric CH4, Optics Express 26, 4, 2018.

Meerdink, S. K., Hook, S. J., Roberts, D. A., and Abbott, E. A.: The ECOSTRESS spectral library version 1.0, Remote Sensing of Environment, 230, 111196, 2019.

Nemtchinov, V., Sun, C., Varanasi, P.: Measurements of Line Intensities and Line Widths in the ν3-fundamental Band of Nitrous Oxide at Atmospheric Temperatures, J. Quant. Spectrosc. Radiat. Transfer 83, 267-284, 2004.

Ngo, N.H., Lisak, D., Tran, H., and Hartmann, J.-M.: An isolated line-shape model to go beyond the Voigt profile in spectroscopic databases and radiative transfer codes, J. Quant. Spectrosc. Radiat. Transfer, 129, 89–100, doi:10.1016/j.jqsrt.2013.05.034, 2013.

Robinson, R., Gardiner, T., Innocenti, F., Woods, P., and Coleman, M.: Infrared differential absorption Lidar (DIAL) measurements of hydrocarbon emissions, J. Environ. Monit., 13, 2213-2220, doi:10.1039/C0EM00312C, 2011.

Spiers, G. D., Menzies, R. T., Jacob, J., Christensen, L. E., Phillips, M. W., Choi, Y., and Browell, E. V.: Atmospheric CO2 measurements with a 2 µm airborne laser absorption spectrometer employing coherent detection, Appl. Opt. 50, 2098-2111, doi: 10.1364/AO.50.002098, 2011.

Stull, R.: Practical Meteorology: An Algebra-based Survey of Atmospheric Science, version 1.02b, Univ. of British Columbia, 940 pages, ISBN 978-0-88865-283-6, 2017.

Sun, X., Abshire, J. B., Beck, J. D., Mitra, P., Reiff, K., and Yang, G.: HgCdTe avalanche photodiode detectors for airborne and spaceborne lidar at infrared wavelengths, Opt. Express 25, 16589-16602, doi:10.1364/OE.25.016589, 2017.

Tian, H., et al.: Global nitrous oxide budget 1980-2020, Earth System Science Data, doi:10.5194/essd-2023-401, 2024.

https://doi.org/10.5194/egusphere-2024-2084
Preprint. Discussion started: 23 July 2024

Vaughan, J. M., Brown, D. W., Nash, C., Alejandro, S. B., and Koenig, G. G.: Atlantic Atmospheric Aerosol Studies: 2. Compendium of Airborne Backscatter Measurements at 10.6 μm, J. Geophys. Res. - Atm., 100 (D1), 1043-1065, doi 10.1029/94JD01817, 1995.

Vaughan, J. M., Geddes, N. J., Flamant P. H., and Flesia, C.: Establishment of a backscatter coefficient and atmospheric database, DERA Report for ESA Contract no. 12510/97/NL/RE, DERA/EL/ISET/CR980139/1.0, 1998.

Waldmann, P., et al.: Quantifying agricultural CH4 and N2O emissions of the Netherlands using a novel airborne eddy-covariance measurements system: First results of the GHGMon campaign in June 2023, EGU24-19467 General Assembly of the European Geosciences Union, Vienna, April 2024.

WMO, 2024: https://wmo.int/activities/global-greenhouse-gas-watch-g3w

Yu, S., Guo, K., Li, S., Han, H., Zhang, Z., and Xia, H.: Three-dimensional detection of CO2 and wind using a 1.57 μm coherent differential absorption lidar, Opt. Express 32, 21134-21148, 2024.